


SCIENTIFIC REPORTS

OPEN

AEO7 Surfactant as an Eco-Friendly Corrosion Inhibitor for Carbon Steel in HCl solution

Mostafa H. Sliem¹, Mohammed Afifi², A. Bahgat Radwan¹, Eman M. Fayyad^{1,3},
Mohamed F. Shibl⁴, Fakiha El-Taib Heikal² & Aboubakr M. Abdallah¹ 

The impact of AEO7 surfactant on the corrosion inhibition of carbon steel (C-steel) in 0.5 M HCl solution at temperatures between 20 °C and 50 °C was elucidated using weight loss and different electrochemical techniques. The kinetics and thermodynamic parameters of the corrosion and inhibition processes were reported. The corrosion inhibition efficiency (*IE*%) improved as the concentration of AEO7 increased. In addition, a synergistic effect was observed when a concentration of 1×10^{-3} mol L⁻¹ or higher of potassium iodide (KI) was added to 40 μmol L⁻¹ of the AEO7 inhibitor where the corrosion *IE*% increased from 87.4% to 99.2%. Also, it was found that the adsorption of AEO7 surfactant on C-steel surface followed the Freundlich isotherm. Furthermore, electrochemical impedance spectroscopy (EIS) and potentiodynamic polarization measurements indicated that AEO7 was physically adsorbed on the steel surface. The surface topography was examined using an optical profilometer, an atomic force microscope (AFM), and a scanning electron-microscope (SEM) coupled with an energy dispersion X-ray (EDX) unit. Quantum chemical calculations based on the density functional theory were performed to understand the relationship between the corrosion *IE*% and the molecular structure of the AEO7 molecule.

Carbon steel (C-steel) is extensively utilized as a construction material in different industrial fields due to its high mechanical properties and low cost. It exists in most industrial infrastructures such as heat exchangers, reactors, drums, boilers and tubings^{1,2}. In oil and gas industries, sulfuric and hydrochloric acids are commonly utilized as pickling acids for the oil wells acidification and the removal of undesirable scales such as rust or mill-scale from steel or any ferrous alloys at elevated temperatures. However, pickling acids are highly corrosive and their aggressiveness needs to be suppressed by adding suitable corrosion inhibitors in small ranges³⁻⁵. For these reasons, an intensive attention is paid for the corrosion of steel in different aggressive corrosion media⁶⁻¹¹. Excellent corrosion inhibition properties are exhibited using inhibitors comprising electronegative atoms such as oxygen, sulfur, phosphorous and/or nitrogen as well as aromatic rings. Recently, eco-friendly biodegradable natural materials show perfect corrosion inhibition efficiencies as well as cost effectiveness. For instance, polymers, possessing polar functional groups such as hydroxyl, carboxylic and amino groups, manifest good corrosion inhibition in different corrosive media because they have a high affinity towards metallic surfaces¹²⁻¹⁶. For decades, surfactants are used in an extensive range of applications, from cleaning purposes such as shampoos, soap and detergents to industrial uses, namely, additives in coatings, concrete mixtures and paints. Moreover, researchers investigate the surfactant-flooding phenomenon in order to enhance the oil recovery. Furthermore, surfactants are utilized as corrosion inhibitors for several metals in the oil and gas production¹⁷⁻²⁰. There are four types of surfactants: anionic, cationic, nonionic and amphoteric. The ethoxylated fatty alcohols surfactants are one of the most common nonionic surfactants that are used in the detergent industry and for an eco-friendly applications^{21,22}. Nevertheless, their corrosion inhibition effectiveness is not yet well exploited especially in acidic environments^{23,24}. For instance, Abdallah has investigated the effect of the numbers of ethylene oxide units of ethoxylated fatty alcohols, on the corrosion of zinc in 0.5 M HCl. It was found that to the corrosion inhibition increase with increasing the concentration and the number of ethylene oxide units per molecule. Inhibition was

¹Center for Advanced Materials, Qatar University, Doha, P.O. Box 2713, Qatar. ²Chemistry Department, Faculty of Science, Cairo University, Giza, 12613, Egypt. ³Physical Chemistry Department, National Research Centre, Dokki, Cairo, Egypt. ⁴Chemistry Department, College of Arts and Sciences, Qatar University, Doha, P.O. Box 2713, Qatar. Correspondence and requests for materials should be addressed to M.F.S. (email: mfshibl@qu.edu.qa) or A.M.A. (email: abubakr_2@yahoo.com)

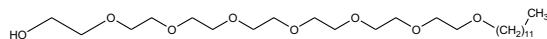


Figure 1. The chemical structure of the AEO7 molecule.

explained on the basis of adsorption of ethoxylated fatty alcohols molecules on the metal surface through their ethoxy groups²⁵. Additionally, a novel eco-friendly Gemini surfactant is synthesized by Mobin *et al.*, namely, Ethan-1,2-diyl bis(N,N-dimethyl-N-hexadecyl ammonium acetoxy) dichloride (16-E2-16). This mixed-type corrosion inhibitor considerably increases the corrosion inhibition efficiency (*IE%*) of mild steel to 98% in 1 M HCl at 60 °C²⁶. Furthermore, three novel nonionic dithiol surfactants are synthesized based on 2-mercaptoacetic acid and polyethylene glycol with different molecular weights to obtain the di-mercaptoethanoate polyethylene glycol: SH600, SH1000 and SH1500. It is proved that the corrosion *IE%* increases with the molecular weight²⁷. The combination of cetyl trimethyl ammonium bromide (CTAB) and indigo carmine significantly enhances the corrosion *IE%* of indigo carmine/CTAB for C-steel to 98.5% at 5×10^{-5} M in 0.5 M HCl²⁸. In addition, a new green inhibitor extracted from *Morus alba pendula* leaves (MAPLE) is used. The corrosion *IE%* increases from 93% at a concentration of 0.4 g L^{-1} to 96% after adding 1 mM of KI²⁹. Moreover, ionic liquids e.g. tetra-*n*-butyl ammonium methioninate is used as a corrosion inhibitor owing to their electrostatic interaction with the iron surface (following Freundlich isotherm) with a maximum efficiency of 93.8% at 1.59×10^{-3} M of the inhibitor in 1 M HCl³⁰. The aim of this work is to investigate AEO7 nonionic surfactant as an eco-friendly corrosion inhibitor for C-steel at ambient and elevated temperatures in 0.5 M HCl, which to the best of our knowledge, has not been previously reported literature. In addition, the adsorption isotherm and the thermodynamic parameters for the adsorption of the AEO7 inhibitor molecules on the C-steel surface are calculated. Furthermore, the synergistic effect of various concentrations of KI on the corrosion *IE%* of AEO7 for C-steel are studied. Moreover, quantum chemical parameters based on the density functional theory method are investigated. For example, the energies of the lowest unoccupied molecular orbitals (E_{LUMO}) and the highest occupied molecular orbitals (E_{HOMO}) as well as the energy gap (ΔE) are calculated. Moreover, the electron affinity (*A*), the ionization potential (*I*), the electronegativity (*X*), the global softness (δ), the dipole moment (μ) and the global hardness (γ) are figured out to provide a theoretical explanation for the corrosion inhibitive behavior of AEO7 and to understand the relation between the corrosion *IE%* and its molecular structure.

Experimental

Materials. C-steel sheets were supplied by Qatar Steel Co., Ltd, Qatar. The chemical composition of C-steel is AISI 1020 alloy of iron and 0.2% carbon with up to 0.7% manganese, 0.65% silicon, and 0.65% copper in wt.%. Steel specimens were abraded to a 4000-grit finish using silicon papers, degreased in acetone, washed with deionized water, and dried in air. The 0.5 M HCl aggressive medium was prepared by diluting an analytical grade 37% HCl with deionized water. The AEO7 surfactant was obtained from Shanghai Dejun Technology Co., Ltd, China. The chemical structure of the surfactant is shown in Fig. 1. Different concentrations of AEO7 (10, 15, 17, and 20 ppm which correspond to 20, 30, 35, and $40 \mu\text{mol L}^{-1}$, respectively) were prepared in deionized water and used as inhibitors for C-steel corrosion in 0.5 M HCl. KI was purchased from Sigma-Aldrich Chemie GmbH (Munich, Germany) to prepare solutions with and without AEO7 in which concentration were (1, 2.5, 5, 7.5, and $10 \times 10^{-3} \text{ mol L}^{-1}$).

Weight loss measurements. The C-steel sheets with dimensions $2.5 \times 2.0 \times 0.2 \text{ cm}^3$ were used for weight loss measurements. The weight loss measurements were performed in a 200 mL glass beaker containing 100 mL of 0.5 M HCl with and without adding different concentrations of AEO7 at room temperature. In order to investigate the effect of time on the rate of corrosion in the presence of the inhibitor, the performance was tested in a range from 30 min to 3 h. Afterwards, the specimens were removed and treated according to the method described in the ASTM G1-90 standard³¹. The corrosion rate (mpy) was computed based on Equation (1).

$$\text{Corrosion rate (mpy)} = \frac{534 W}{\rho A t} \quad (1)$$

where *W* is mass loss in mg, ρ is the C-steel density in g cm^{-3} , *A* is the surface area of the sample in cm^2 and *t* is the time of the test in h.

The corrosion *IE%* and the surface coverage θ of the inhibitor used for the corrosion of C-steel were calculated as follows^{15,32},

$$IE\% = \theta \times 100 = \frac{(W^0 - W)}{W^0} \times 100 \quad (2)$$

where W^0 and *W* are the average weight loss values without and with adding the inhibitor, respectively.

Electrochemical measurements. Electrochemical measurements were performed in a three-electrode double-jacketed cell. The C-steel working electrodes were prepared according to the aforementioned procedures described in Section 2.1. It had an exposed area of 0.5 cm^2 . A graphite sheet with the same exposed area was used as a counter electrode and a saturated calomel electrode (SCE) acted as a reference electrode. The reference electrode was coupled with a Luggin capillary to minimize the *IR* potential drop. A Julabo F12 thermostat (GmbH, Seelach, Germany) was utilized to control the temperature of the solution as all electrochemical tests

were carried out at various temperatures (20 °C, 30 °C, 40 °C, and 50 °C) in the presence and absence of different concentrations of the inhibitor. Before any electrochemical measurement, the C-steel electrode was dipped in the solution for 30 minutes to achieve a steady state condition. The EIS analyses were performed under an open circuit potential (OCP) condition within a frequency range of 0.1 Hz to 100 kHz with an AC amplitude of 10 mV using a GAMRY 3000 potentiostat/galvanostat/ZRA (Warminster, PA, USA). The potentiodynamic cathodic and anodic polarization curves varied from -250 mV to +250 mV versus open circuit potential (OCP) with a scan rate of 0.3 mV s⁻¹. To ensure reproducibility, each test was repeated three times.

Surface morphology. The surface of C-steel was examined using different characterization techniques. A Leica optical profilometer was utilized to explore the surface topography and surface roughness at a microscale. At the same time, an Asylum Research MFP-3D, atomic force microscope, AFM (Santa Barbara, CA, USA) was used to measure the surface roughness and surface topography in nanoscale and compared to the results that were obtained from the optical profilometer. The surface condition was checked using an FEI NOVA NANOSEM 450 high field emission scanning electron microscope, HFSEM, (Hillsboro, OR, USA) to document the corrosion of C-steel.

Computational. A quantum chemical study was carried out using the density functional theory (DFT) method as implemented in the GAUSSIAN09 suit of programs³³. Geometric optimization was performed using the B3LYP functional combined with the cc-pvdz basis set. The B3LYP functional (with Becke's three-parameter functional (B3) and a mixture of HF with DFT exchange terms linked to the gradient-corrected correlation functional of Lee, Yang, and Parr (LYP)^{34,35}) is known to produce a good estimate of molecular properties related to reactivity. The consistent-correlated polarized valence double zeta basis set (cc-pvdz) basis set^{36,37} became a state of the art for correlated calculations. The DFT, among other functions, seems promising for revealing changes in the electronic structure responsible for the inhibitory action of compounds on metal surfaces. The geometry of AEO7 was fully optimized using a gradient minimization technique. The optimum structure was characterized as having a zero-gradient norm. By diagonalizing the matrix of the second derivatives, positive harmonic vibrational frequencies were observed. The Gaussian 09 software was utilized to calculate the quantum chemical parameters necessary to explain the atomic and molecular interactions involving the compounds. GaussView 5.0 software was further applied in visualizing the electron density graphical isosurfaces and the quantum chemical parameters, which were calculated in the domain of Koopmans' theory³⁸ such as the energy of the highest occupied molecular orbital (E_{HOMO}) and the energy of the lowest unoccupied molecular orbital (E_{LUMO}). Moreover, the ionization potential (I) and the electron affinity (A) associated with the energies of HOMO and LUMO, respectively, where $I = -E_{\text{HOMO}}$, $A = -E_{\text{LUMO}}$ and the energy gap ($\Delta E = E_{\text{HOMO}} - E_{\text{LUMO}}$), as well as the chemical potential (μ), the absolute hardness (χ), and the absolute softness were calculated.

The global hardness (γ) reflects the resistance to a charge transfer while the global softness (δ) describes the ability to receive electrons and were estimated by:

$$\gamma = -\frac{1}{2}(E_{\text{Homo}} - E_{\text{Lumo}}) \quad (3)$$

$$\delta = \frac{1}{\gamma} \cong -\frac{2}{E_{\text{HOMO}} - E_{\text{LUMO}}} \quad (4)$$

Electronegativity (X) is the power of an atom to attract electrons towards itself and was calculated using Koopmans' theory

$$X = -\frac{1}{2}(E_{\text{Homo}} + E_{\text{Lumo}}) \quad (5)$$

Results and Discussion

Weight loss measurements. *Effect of inhibitor concentration on corrosion of C-steel.* Figure 2 shows the weight loss transients for C-steel upon immersion in 0.5 M HCl in the presence and absence of 20, 30, 35, and 40 $\mu\text{mol L}^{-1}$ of AEO7 at 25 °C. It reveals that the higher the concentration of AEO7 is, the lower the weight loss we measure i.e. the higher the corrosion $IE\%$ we calculate. The result can be attributed to the ability of AEO7 to be adsorbed on the surface of C-steel because of the existence of seven oxygen atoms arranged in a kind of chain sequence in AEO7 which helps the 3d orbitals of an iron atom to interact with the lone pairs of electrons from the oxygen atoms³⁹⁻⁴¹. This, consequently, increases the corrosion $IE\%$. In addition, the high molecular weight of AEO7, because of the presence of a long chain of hydrophobic ethylene groups, increases the corrosion $IE\%$. Therefore, in the presence of AEO7, the corrosion rate is an indicator for the number of free corrosion sites remaining after effectively blocking the other sites by the adsorbed inhibitor molecule^{25,42}.

Effect of immersion time on corrosion of C-steel. Assuming that corrosion takes place only at the free sites while neglecting the corrosion rates of the covered sites, the corrosion $IE\%$ can be calculated by Equation 2. Table 1 shows the results for corrosion $IE\%$ of different concentrations of AEO7 on C-steel after various immersion times at 25 °C. The increase in the corrosion rate with time is attributed to the entanglement of the polymer chains with each other with time which lowers the overall entropy surface energy meanwhile exposes more active sites for corrosion^{43,44}.

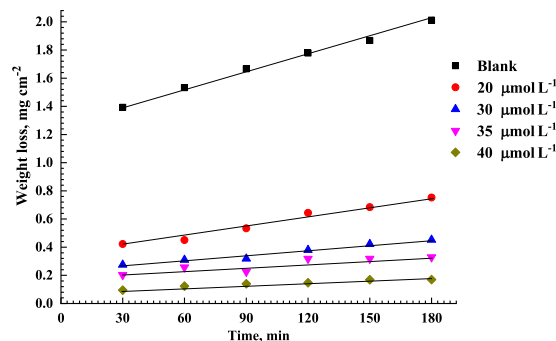


Figure 2. Weight loss transients for C-steel upon immersion in 0.5 M HCl in the presence and absence of 20, 30, 35, and 40 $\mu\text{mol L}^{-1}$ of AEO7 at 25 °C.

C_{inh} ($\mu\text{mol L}^{-1}$)	Corrosion IE%					
	30 min	60 min	90 min	120 min	150 min	180 min
Blank	—	—	—	—	—	—
20	69.7	70.6	67.1	63.8	63.4	62.6
30	80.3	79.8	80.9	78.6	77.4	77.5
35	85.4	83.2	86.4	82.1	82.9	83.7
40	93.2	91.9	91.6	91.7	91.0	91.6

Table 1. Corrosion IE% of AEO7 for the corrosion of C-steel in 0.5 M HCl after different exposure times at 25 °C.

EIS measurements. Figure 3 shows the EIS Nyquist plots for C-steel in 0.5 M HCl solution in the absence and presence of 20, 30, 35 and 40 $\mu\text{mol L}^{-1}$ of the AEO7 corrosion inhibitor. Clearly, the diameters of the semicircles in the presence of AEO7 inhibitor are larger compared to the blank one. It is also lucid that the diameters of the semicircles decrease as the temperature increases at the same concentration of the AEO7 inhibitor. In addition, the depressed capacitive loops at low frequency in all the Nyquist plots refer to a charge transfer-controlled mechanism for the corrosion of C-steel in the 0.5 M HCl solution. The deviation of the capacitive loop from a complete semi-circle can be referred to the heterogeneity and microroughness of the working electrode surface^{45,46}.

Figure S1 (Supporting Information) depicts the Bode plots and phase angle curves for the same EIS data represented by the Nyquist plots shown in Fig. 3. In contrast to the effect of increasing the temperature, raising the AEO7 concentration increases the phase angles and shifts their peaks to lower frequencies^{47–50}. It can be seen that the phase angles for the inhibited cases are much higher than the uninhibited ones. The increased values of the phase angle for the inhibited specimens indicated that the surface becomes smoother owing to the inhibitor adherence to the metallic surface and the formation of a protective film of inhibitors over the metallic surface. The broadening and the shift to lower frequencies of the single maximum in the Bode plots further supports the protective film formation by inhibitor molecules^{51,52}. Figure 4 shows a one-time constant equivalent electrical circuit (EC) that is used for fitting the measured EIS data of a uniformly corroding electrodes in an electrolyte^{53,54}. The EC is composed of an uncompensated solution resistance (R_s), a charge transfer resistance (R_{ct}) and a constant phase element (CPE) that replaces the capacitive element to obtain a more accurate fit. CPE is used for a non-ideal double-layer capacitor. The non-ideal behavior of a double layer can be attributed to many reasons; e.g, surface roughness and a non-uniform (i) surface coverage, (ii) corrosion rate and/or (iii) current distribution.

The impedance of the CPE is expressed by Equation 6⁵⁵:

$$Z_Q = [Y_0^{-1}(j\omega)^{-n}] \quad (6)$$

where Z_Q is CPE impedance ($\Omega \text{ cm}^{-2}$), Y_0 is the CPE constant in $\mu\text{s}^n \text{ ohm}^{-1} \text{ cm}^{-2}$, $j = (-1)^{1/2}$, ω is the angular frequency in rad s^{-1} and the value of n ranges between 0 and 1. When $n = 1$, the CPE becomes equivalent to an ideal capacitor, and when $n = 0$, the CPE becomes equivalent to a resistor. The double layer capacitance (C_{dl}) can be calculated using the following equation⁵⁶:

$$C_{dl} = \frac{(Y_0 R_{ct})^{1/n}}{R_{ct}} = Y_0 \omega^{(n-1)} \quad (7)$$

The surface coverage (θ) is estimated using the following equation:

$$\theta = \frac{R_{ct1} - R_{ct2}}{R_{ct1}} \quad (8)$$

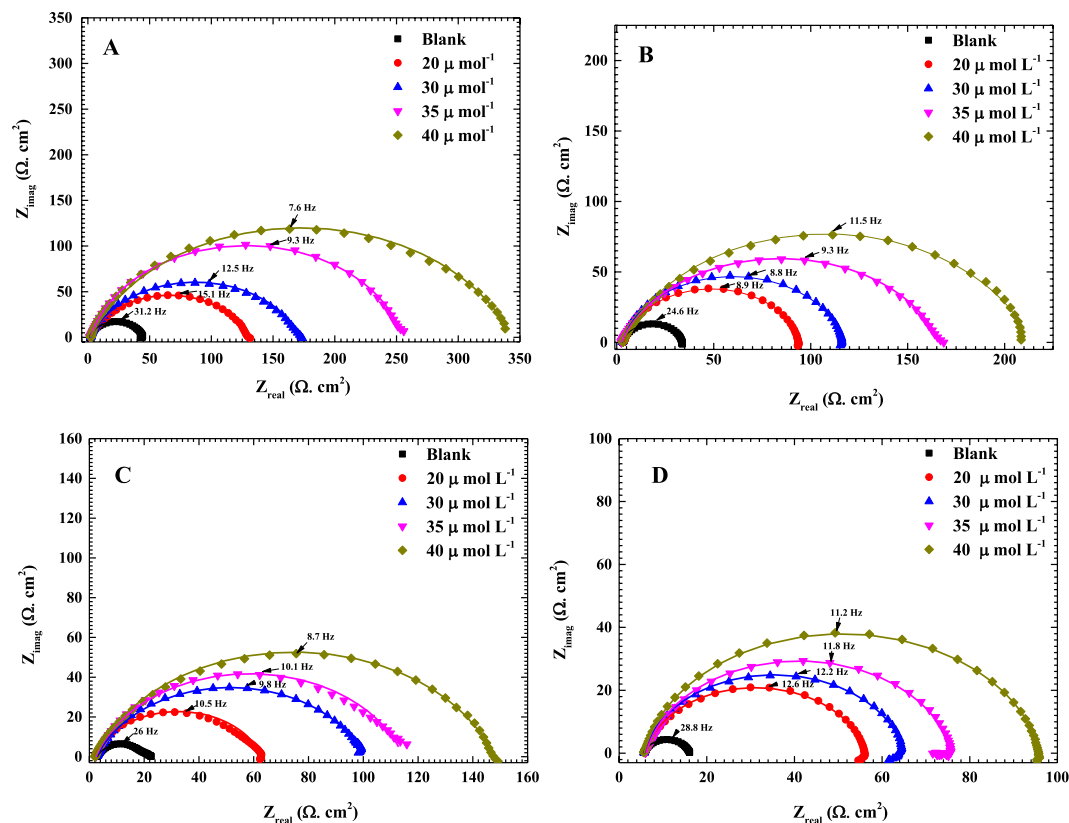


Figure 3. Measured EIS Nyquist plots (dotted) and their fitted curves (solid lines) for C-steel in 0.5 M HCl solution in the presence of 0, 20, 30, 35 and 40 $\mu\text{mol L}^{-1}$ of AEO7 corrosion inhibitor at (A) 20, (B) 30, (C) 40 and (D) 50 $^{\circ}\text{C}$. The fitting is done using the equivalent circuit shown in Fig. 4.

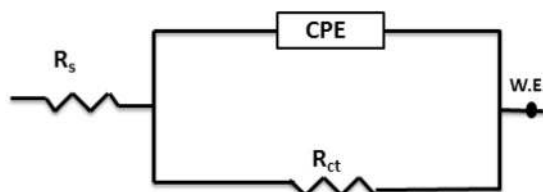


Figure 4. An equivalent electrical circuit used for the analysis of EIS measured data.

where R_{ct1} and R_{ct2} are the charge-transfer resistances in the presence and absence of the inhibitor, respectively. Moreover, the corrosion $IE\%$ is calculated using Equation 2^{55,56}. All EIS parameters obtained from the Nyquist and Bode graphs are summarized in Table 2.

It can be noticed that the higher the concentration of the AEO7 inhibitor is, the larger the charge transfer resistance we measure which is typically opposite to the behavior of the C_{dl} which decreases with increasing the AEO7 concentration or decreasing the temperature^{57,58}. For instance, comparing the blank solution with the one containing 20 $\mu\text{mol L}^{-1}$ of AEO7 at 20 $^{\circ}\text{C}$, the R_{ct} increases from 43 $\Omega\text{ cm}^2$ to 128 $\Omega\text{ cm}^2$, and C_{dl} decreases from 119.75 μF to 82.57 μF ($IE\%$ is 66.4%). Meanwhile, increasing the inhibitor concentration to 40 $\mu\text{mol L}^{-1}$ increases the R_{ct} value to 341.6 $\Omega\text{ cm}^2$, and the C_{dl} decreases to 59.51 μF with an $IE\%$ of 87.6%. This observation can be explained using the Helmholtz equation⁵⁵.

$$\delta_{ads} = \frac{\epsilon\epsilon_0 A}{C_{dl}} \quad (9)$$

where δ_{ads} is the thickness of the adsorbed layer of the AEO7 corrosion inhibitor, ϵ_0 is the vacuum permittivity, ϵ is the local relative dielectric constant and A is the area of C-steel electrode. This equation shows that C_{dl} is inversely proportional to δ_{ads} i.e. the decrease of the C_{dl} value is attributed to the growth of the adsorbed film of AEO7 corrosion inhibitor as its concentration increases in solution. As the protective film grows, the charge transfer becomes more sluggish as indicated by the high R_{ct} and corrosion $IE\%$ values. Increasing the temperature

T (°C)	C _{inh} μmol L ⁻¹	R _{ct} Ω cm ²	CPE			θ	Corrosion IE%
			Y ₀ μs ⁿ ohm ⁻¹ cm ⁻²	C _{dl} μF	n		
20	Blank	43.1	257.0	119.7	0.855	—	—
	20	128.2	211.7	82.57	0.793	0.664	66.4
	30	169.8	194.5	76.85	0.786	0.746	74.6
	35	253.0	161.4	69.31	0.791	0.830	83.0
	40	341.6	105.95	59.49	0.852	0.874	87.4
30	Blank	30.8	381.8	218.7	0.889	—	—
	20	90.42	314.1	202.2	0.890	0.660	66.0
	30	114.2	260.4	156.8	0.874	0.730	73.0
	35	164.5	236.8	103.6	0.797	0.813	81.23
	40	211.5	149.2	64.25	0.804	0.854	85.4
40	Blank	24.27	425.0	252.7	0.898	—	—
	20	64.8	405.7	231.0	0.866	0.625	62.5
	30	89.0	390.3	185.7	0.819	0.727	72.7
	35	112.2	377.0	141.9	0.764	0.786	78.6
	40	145.8	331.4	124.6	0.756	0.833	83.3
50	Blank	18.5	606.5	295.6	0.862	—	—
	20	49.27	554.2	254.1	0.822	0.622	62.2
	30	59.32	543.7	217.4	0.789	0.688	68.8
	35	69.72	515.7	187.7	0.890	0.734	73.4
	40	90.42	492.8	155.0	0.729	0.795	79.5

Table 2. EIS parameters and corrosion inhibition efficiencies obtained from fitting impedance spectra of C-steel in 0.5 M HCl at different concentrations of AEO7 at 20, 30, 40 and 50 °C using the electrical equivalent circuit shown in Fig. 4.

will decrease the corrosion IE% because the desorption rate of the inhibitor molecules from the C-steel surface increases which leads to an increase in the dissolution rate of the steel⁵⁹.

In general, the higher the inhibitor concentration is, the less positive the n values are. This indicates that the behavior of the constant phase element is becoming farther from the ideal capacitor as the AEO7 concentration increases^{60,61}.

Potentiodynamic polarization measurements. Figure 5 shows the potentiodynamic polarization curves of the C-steel in a 0.5 M HCl solution at a scan rate of 0.3 mV s⁻¹ in the presence of 0, 20, 30, 35 and 40 μmol L⁻¹ of AEO7 corrosion inhibitor at (A) 20, (B) 30, (C) 40 and (D) 50 °C. The electrochemical kinetic parameters such as the corrosion free potential (E_{corr}), corrosion current density (i_{corr}), the polarization resistance (R_p) and the cathodic and anodic Tafel slopes (β_c and β_a , respectively) which are obtained by the Tafel extrapolation method are listed in Table 3. The corrosion rates are calculated using Equation 10 assuming that the whole surface of the C-steel is attacked by the aggressive media, and no localized corrosion is detected^{62,63}.

$$\text{corrosion rate(mm/year)} = \frac{i_{\text{corr}} * 10 * M * 3.15 * 10^7}{F * n * d} \quad (10)$$

$3.15 * 10^7$ is the number of seconds in one year and 10 is a factor to change cm to mm. M is the atomic weight of iron (g mol⁻¹) while n is the number of transferred electrons per metal atom, F is Faraday's constant (96497 C mol⁻¹), A is the exposed area of the electrode, d is the density of iron, and i_{corr} is the corrosion current density in A cm⁻².

The polarization resistance (R_p), can be calculated using the Stern–Geary equation⁵⁵.

$$R_p = \frac{\beta_c \beta_a}{2.303 i_{\text{corr}} (\beta_c + \beta_a)} \quad (11)$$

The values of surface coverage (θ) are calculated using the following equation:

$$\theta = \frac{i'_{\text{corr}} - i_{\text{corr}}}{i'_{\text{corr}}} \quad (12)$$

where i'_{corr} and i_{corr} are the corrosion current densities in the absence and presence of the AEO7 corrosion inhibitor. In addition, the corrosion IE% is calculated using Equation 2⁵⁵.

It is worth noting that the presence of AEO7 corrosion inhibitor decreases the anodic and cathodic current densities and the corrosion potentials are shifted towards the nobler direction compared to the blank. This is a typical behavior for the mixed-type corrosion inhibitors⁶⁴. It is reported that an inhibitor to be considered as cathodic or anodic one requires a shift of ±85 mV in the E_{corr} between the uninhibited and inhibited systems,

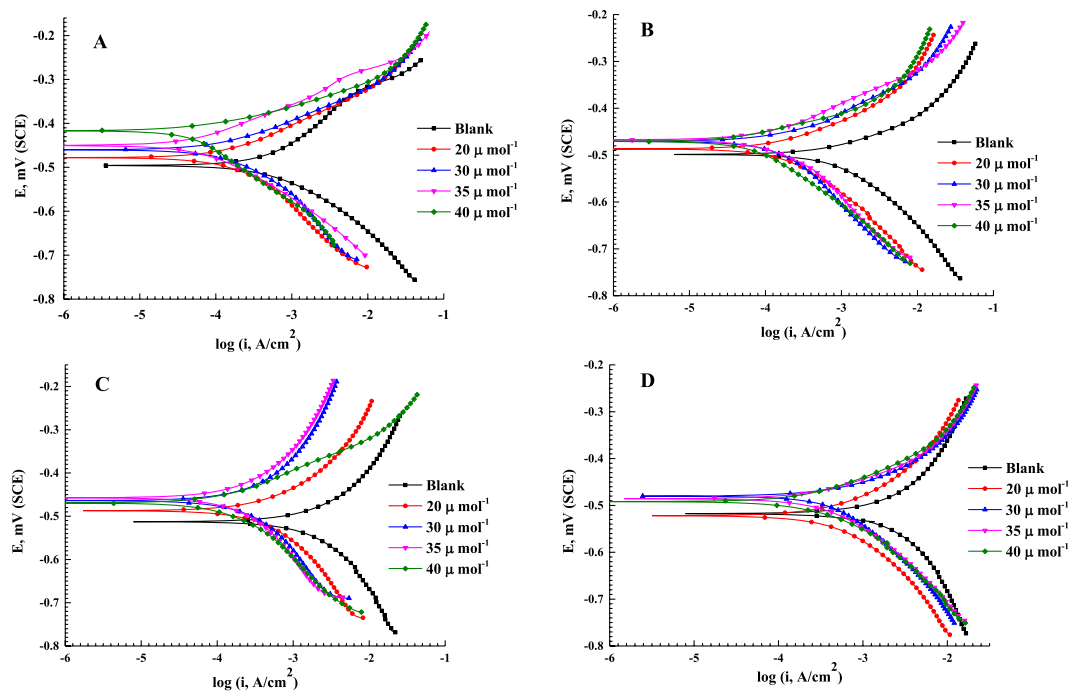


Figure 5. Potentiodynamic polarization curves for C-steel at a scan rate of 0.3 mV s^{-1} in 0.5 M HCl in the presence of $0, 20, 30, 35, 40 \mu\text{mol L}^{-1}$ of AEO7 corrosion inhibitor at (A) 20, (B) 30, (C) 40 and (D) 50°C .

T ($^\circ\text{C}$)	$C_{\text{inh}} \mu\text{mol L}^{-1}$	$-E_{\text{corr}}$ (mV SCE)	i_{corr} ($\mu\text{A cm}^{-2}$)	β_a , mV decade $^{-1}$	β_c , mV decade $^{-1}$	R_p , $\Omega \text{ cm}^2$	CR, mm year $^{-1}$	θ	IE %
20	Blank	496.0	624	152.8	164.8	55.2	7.24	—	—
	20	478.0	194	97.2	157.9	130.1	2.25	0.68	68.91
	30	460.0	130	87.8	148.6	199.9	1.5	0.80	80.40
	35	458.0	71.5	68.1	123.6	266.9	0.83	0.88	88.54
	40	417.0	45.5	40.1	112.6	282.5	0.52	0.92	92.70
30	Blank	499.0	1056	202.2	192.8	40.6	12.26	—	—
	20	487.0	353.68	122	173.3	88.01	4.1	0.66	66.5
	30	471.0	250.9	107.5	162.9	127.9	2.91	0.79	79.3
	35	467.0	150.4	85.5	148.5	156.8	1.74	0.85	85.75
	40	470.0	95.8	56.8	129	178.9	1.11	0.90	90.92
40	Blank	513.0	1640	249.5	328.4	37.5	19.04	—	—
	20	487.0	567	211.2	272.1	91.1	6.58	0.65	65.42
	30	464.0	419	183.5	250.5	122.1	4.86	0.77	77.45
	35	457.0	277	149.5	225.7	141.1	3.21	0.83	83.10
	40	469.0	166	93.8	143.9	148.7	1.92	0.89	89.87
50	Blank	518.0	2440	423	352	34.2	28.34	—	—
	20	522.0	896	281	323.9	73.0	10.4	0.63	63.27
	30	480.0	650	183.1	285.3	80.8	7.54	0.75	75.36
	35	486.0	425	98.1	260.6	68.8	4.93	0.81	81.70
	40	492.0	301	44.9	235.3	54.4	3.49	0.78	87.66

Table 3. Potentiodynamic polarization parameters (derived from Fig. 5) for C-steel in 0.5 M HCl in the presence of $0, 20, 30, 35, 40 \mu\text{mol L}^{-1}$ of AEO7 corrosion inhibitor at different temperatures.

otherwise it is classified as a mixed type one^{44,65}. The E_{corr} values, in Table 3, confirm that AEO7 is of the mixed type category. The higher the concentration of the AEO7 is, the lower the corrosion rates are at any temperature. This can be explained by the increase in the local electron density at the steel surface by which the affinity of C-steel towards the adsorption of negatively charged Cl^- ions decreases and consequently the corrosion rate is lowered. On the other hand, raising the temperature increases the corrosion rate at the same concentration of the AEO7 due to the increase in the desorption rate of the corrosion inhibitor from the C-steel surface⁶⁶. It is worth mentioning that the polarization data shown in Fig. 5 confirm the EIS ones in Figs 3 and S1.

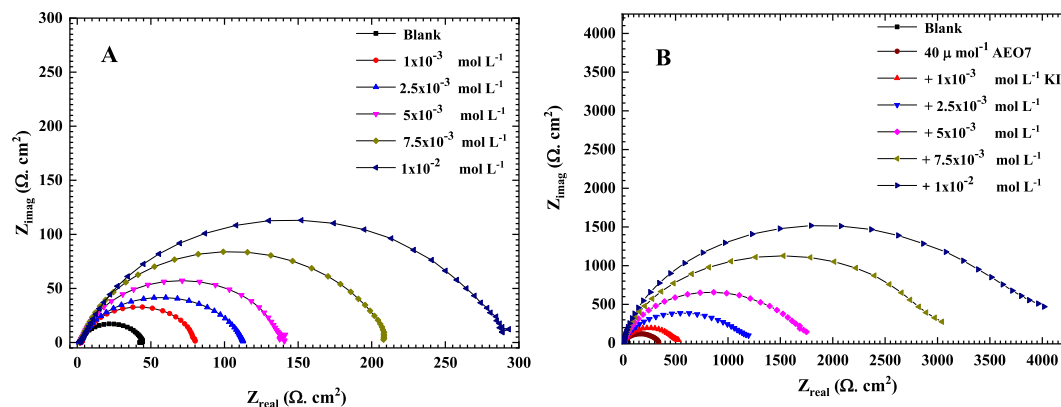


Figure 6. EIS Nyquist plots for C-steel in 0.5 M HCl at 20 °C with 0, 1, 2.5, 5, 7.5, 10×10^{-3} M of KI in the (A) absence and (B) presence of $40 \mu\text{mol L}^{-1}$ of AEO7. Solid lines are the fittings that are done using the equivalent circuit shown in Fig. 4 while the symbols are the measured data.

C_{inh} , mol L ⁻¹	R_{ct} , Ω cm ²	CPE			θ	Corrosion IE%
		$Y_0 \times 10^{-6} \text{ s}^n \text{ ohm}^{-1} \text{ cm}^{-2}$	C_{dl} , μF	n		
Blank	43.1	257.0	119.7	0.855	—	—
AEO7	341.6	105.95	67.91	0.852	0.87	87.4
1×10^{-3}	493	63.98	42.10	0.892	0.913	91.3
2.5×10^{-3}	1196	51.08	37.31	0.899	0.963	96.3
5×10^{-3}	1973	52.45	34.81	0.847	0.978	97.8
7.5×10^{-3}	3250	48.70	32.58	0.821	0.986	98.6
1×10^{-2}	4351	24.61	9.73	0.719	0.992	99.2

Table 4. The electrochemical parameters and corrosion inhibition efficiencies obtained from the measured impedance spectra of C-steel in 0.5 M HCl at different concentrations of KI with $40 \mu\text{mol L}^{-1}$ of AEO7 at room temperature.

Synergism Analysis. Figure 6 illustrates the EIS Nyquist plots of C-steel in 0.5 M HCl at 20 °C in the presence of (0, 1, 2.5, 5, 7.5, 10) $\times 10^{-3}$ mol L⁻¹ KI (A) without and (B) with $40 \mu\text{mol L}^{-1}$ of AEO7 corrosion inhibitor. It is clear that the diameters of the semicircles increase as the concentration of KI increases (compare the plots in Fig. 6B). The maximum efficiency of AEO7 corrosion inhibitor increases from 87.4 in the absence of KI to 99.2% in the presence of 1×10^{-2} mol L⁻¹ of it. It is reported that the addition of halide ions to the corrosion inhibitors can, synergistically, enhance the corrosion inhibition efficiencies in aggressive media^{28,57,67–69}. The iodide ions compete with the chloride ions for getting adsorbed on the steel surface then the AEO7 corrosion inhibitor molecules are attracted to the adsorbed iodide ions electrostatically as iodide ions increase the adsorbability of the AEO7 by forming interconnecting bridges between the C-steel surface and the inhibitor molecules^{67,68}. Tables 4 and S1 summarize the results of the corrosion inhibition measurements and calculations for C-steel in 0.5 M HCl in the presence of different concentrations of KI with and without $40 \mu\text{mol L}^{-1}$ of AEO7.

To determine the synergistic effect of KI, the synergism parameter S_1 is calculated using Aramaki and Hackerman's Equation⁷⁰:

$$S_1 = \frac{1 - \theta'_{1+2}}{1 - \theta'_{1+2}} \quad (13)$$

where $\theta'_{1+2} = (\theta_1 + \theta_2) - (\theta_1 \times \theta_2)$, θ'_{1+2} represents the measured surface coverage for a certain concentration of KI in combination with a $40 \mu\text{mol L}^{-1}$ of AEO7, θ_1 is the surface coverage of KI at a certain concentration and θ_2 is the surface coverage of $40 \mu\text{mol L}^{-1}$ AEO7. The synergistic effect of KI with other inhibitors is common. However, in this research the interaction between KI and AEO7 is changing according to the concentration of iodide ions as seen in Table 5. Three conditions are reported with altering the KI concentration leading to different S_1 values. If S_1 values are more than unity, then the synergistic effect of KI is proved. However, if S_1 values approach unity, it means that there is no interaction between potassium iodide and the AEO7 molecule. If S_1 values are less than unity, an antagonistic behavior is expected which is a characteristics of a competitive adsorption process^{69,71,72}. The synergism is originated from the double role that iodide ions play. The protective iodide ions compete with the chloride corrosive ones for the adsorption on the surface of the metal and at the same time they increase the adsorbability of AEO7 molecules on the C-steel surfaces^{43,44}. Table 5 shows the values of S_1 that are calculated after the addition of different concentrations of KI to a 0.5 M HCl solution with $40 \mu\text{mol L}^{-1}$ of AEO7. It is evident

C, mol L ⁻¹ (KI)	S ₁
1 × 10 ⁻³	0.672
2.5 × 10 ⁻³	1.230
5 × 10 ⁻³	1.773
7.5 × 10 ⁻³	1.857
1 × 10 ⁻²	1.773

Table 5. Calculated synergistic parameter S₁ for different concentration of KI for C-steel in 0.5 M HCl in the presence of 40 μmol L⁻¹ of AEO7 corrosion inhibitor at 20 °C.

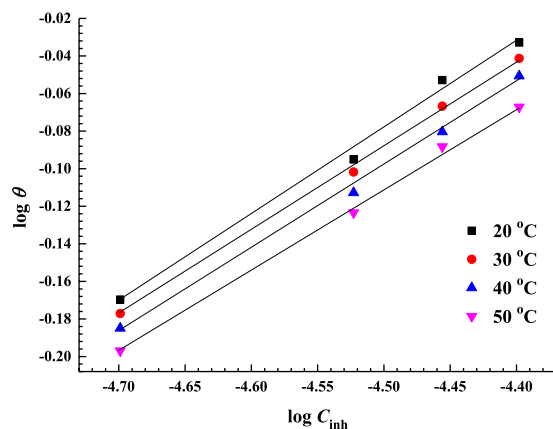


Figure 7. Freundlich isotherm plots for the adsorption of AEO7 on C-steel in 0.5 M HCl at different temperatures.

that the values are greater than unity for all KI concentrations that are higher than 1 × 10⁻³ M which proves the synergism between KI and AEO7.

Inhibitor Adsorption and thermodynamic analysis. The equilibrium constants for the adsorption of AEO7 on the C-steel surface in a 0.5 M HCl solution at different temperatures can be derived from the proper adsorption isotherm. Freundlich adsorption isotherm shows the best fitting for the surface coverage of AEO7 on C-steel with its concentration in solution⁷³. This isotherm can be summarized by Equations 14 and 15, as given below:

$$\theta = K_{\text{ads}} C^n \quad (14)$$

$$\log \theta = \log K_{\text{ads}} + 2.303 n \log C \quad (15)$$

where C is the concentration of the corrosion inhibitor, K_{ads} is the equilibrium constant for the adsorption process and θ is the surface coverage (obtained from the potentiodynamic polarization analysis shown in Table 3) while n is a function in the strength of adsorption.

Equation 15 is used to create Fig. 7 at various temperatures. R^2 values are close to unity confirming the properness of using the Freundlich isotherm^{30,74}. From the intercepts of the graphs, K_{ads} values are computed. K_{ads} constants are also used to calculate the values of the standard Gibbs free energy change of adsorption $\Delta G_{\text{ads}}^{\circ}$ according to the following Equation^{75,76}

$$\Delta G_{\text{ads}}^{\circ} = -RT \ln(55.5 K_{\text{ads}}) \quad (16)$$

where R is the universal gas constant in J mol⁻¹ K⁻¹, T is the temperature in K and 55.5 is the number of moles of water per liter, according to Boukhalah *et al.*⁷⁷. Calculated values of R^2 , K_{ads} and $\Delta G_{\text{ads}}^{\circ}$ are listed in Table 6. In addition, the enthalpy change of adsorption, $\ln K_{\text{ads}}$, was plotted versus $1/T$, which resulted in a straight line, as shown in Fig. 8, following the Van't Hoff equation.

There are different types of adsorption that represent the interaction between the metal surface and the corrosion inhibitor molecule e.g. physical, chemical or chemi/physorption. From the results in Table 6, $\Delta G_{\text{ads}}^{\circ}$ are negative and the absolute values are in the range of 20.94–22.22 kJ mol⁻¹. Generally, if $\Delta G_{\text{ads}}^{\circ} \leq -20$ kJ mol⁻¹, it is linked to physisorption while if it is ≥ -40 kJ mol⁻¹, then it is inclined to chemisorption^{7,60}. In recent reports, $\Delta G_{\text{ads}}^{\circ}$ values in the range from -28 to -38 kJ/mol are interpreted as mixed adsorption (i.e both physisorption and chemisorption)^{61,63}. The $\Delta G_{\text{ads}}^{\circ}$ values obtained in the present investigation fall close to the category of the physisorption type of adsorption.

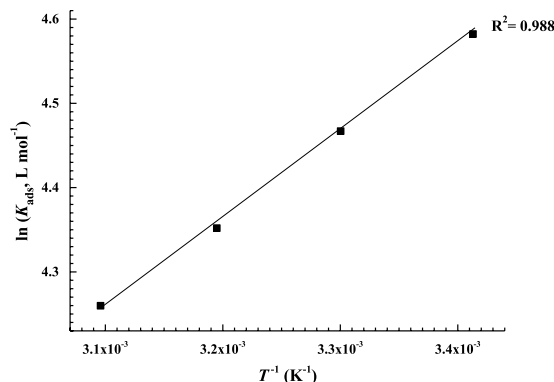


Figure 8. Van't Hoff plot for the AEO7 corrosion inhibitor on C-steel surface in 0.5 M HCl at different temperatures.

Temperature, K	K_{ads}	R^2	ΔG_{ads}° (kJ mol ⁻¹)	ΔH_{ads}° (kJ mol ⁻¹)	ΔS_{ads}° (J. mol ⁻¹ K ⁻¹)
293.15	97.723	0.995	-20.94	-8.90	41.00
303.15	87.096	0.998	-21.37	-8.90	41.15
313.15	77.624	0.990	-21.78	-8.90	41.44
323.15	70.795	0.994	-22.22	-8.90	41.30

Table 6. Thermodynamic parameters derived and calculated based on Freundlich adsorption isotherms and polarization measurements.

K_{ads} values are often used to describe the strength of the bond between adsorbent and adsorbate⁶³. It can be seen in Table 6 that increasing the temperature decreases the K_{ads} as the bonds between C-steel and AEO7 molecules are weakened.

ΔG_{ads}° is connected to ΔH_{ads}° (standard enthalpy) and ΔS_{ads}° (standard entropy) of adsorption according to Equation 17:

$$\Delta G_{ads}^{\circ} = \Delta H_{ads}^{\circ} - T\Delta S_{ads}^{\circ} \quad (17)$$

Combining and rearranging Equations 16 and 17 lead to the Van't Hoff Equation below (Equation 18)

$$\ln K_{ads} = \frac{-\Delta H_{ads}^{\circ}}{RT} + \frac{\Delta S_{ads}^{\circ}}{R} - \ln 55.5 \quad (18)$$

ΔH_{ads}° is obtained from the slope of the Van't Hoff plot and ΔS_{ads}° is obtained from Equation 17 and listed in Table 6.

The ΔH_{ads}° values can provide a vital information pertaining to the adsorption mechanism of an inhibitor. In the present study, ΔH_{ads}° value is negative implying exothermic adsorption. Similar results are reported by Esmaili *et al.*⁷⁸. The negative value of ΔH_{ads}° value is confirmed by the decrease in the corrosion $IE\%$ with increasing the temperature. On the other hand, the calculated values of ΔS_{ads}° are positive which is attributed to the increase in the solvent energy in addition to the increase in entropy due to H₂O desorption⁷⁹. Noor *et al.* also referred the positive ΔS_{ads}° values to the substitution of several water molecules by a single inhibitor molecule⁸⁰.

Analysis of Corrosion Kinetics. The effect of temperature on the dissolution of C-steel specimen in a 0.5 M HCl solution in the presence and absence of different concentrations of AEO7 is examined between 20–50 °C. Consequently, the corrosion kinetics parameters, namely, E_a (activation energy), ΔH^* (activation enthalpy), and ΔS^* (activation entropy) are calculated from the Arrhenius and transition state equations,

E_a can be calculated using Arrhenius Equation^{81,82}:

$$\log CR = \log A - \frac{E_a}{2.303 RT} \quad (19)$$

where CR stands for the corrosion rate at a temperature (T) which is expressed by the corrosion current density (i), E_a represents the apparent activation energy and A is the Arrhenius constant that depends on the metal type and electrolyte. R is the universal gas constant (8.314 J mol⁻¹ K⁻¹).

Figure 9 shows the relation between $\log i$ and $1/T$ for C-steel in 0.5 M HCl solution with and without AEO7. From the slopes, E_a can be calculated for each concentration.

The activation enthalpy (ΔH^*) and activation entropy (ΔS^*), for the corrosion of C-steel in a 0.5 M HCl with and without AEO7 are calculated from the transition-state equation, as shown by Shuklar *et al.*⁸³.

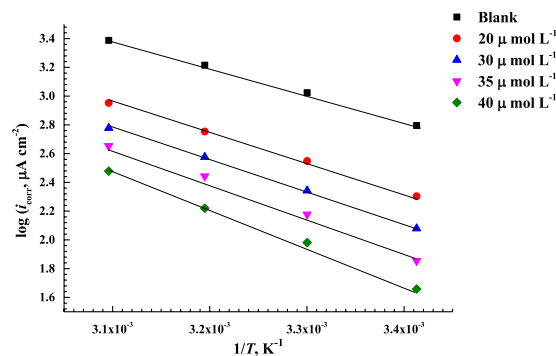


Figure 9. Arrhenius plots for the corrosion current densities ($\log i$) versus $1/T$ at different concentrations of the AEO7 corrosion inhibitor in 0.5 M HCl.

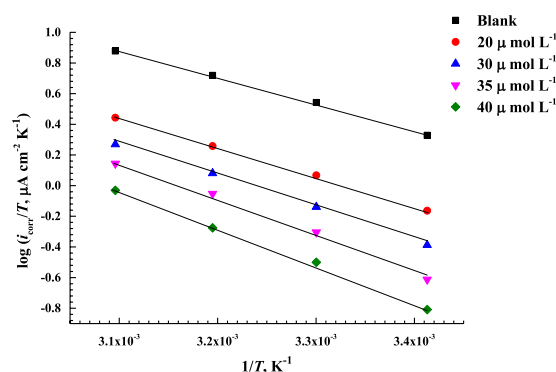


Figure 10. Transition-state plots of $\log(i/T)$ versus $1/T$ for C-steel in 0.5 M HCl with and without different concentrations of AEO7 corrosion inhibitor.

C_{inh} $\mu\text{mol L}^{-1}$	E_a (kJ mol^{-1})	ΔH^* (kJ Mol^{-1})	ΔS^* ($\text{J mol}^{-1} \text{K}^{-1}$)
0	35.70	-33.12	-77.96
20	39.92	-37.31	-73.36
30	42.13	-38.39	-68.94
35	47.05	-44.43	-57.08
40	49.60	-46.40	-54.36

Table 7. Activation energy (E_a), activation enthalpy (ΔH^*) and activation entropy (ΔS^*) for C-steel in 0.5 M HCl with the presence of various concentrations of AEO7 corrosion inhibitors.

$$CR = \frac{RT}{Nh} e^{\frac{\Delta S^*}{R}} e^{-\frac{\Delta H^*}{RT}} \quad (20)$$

where CR is the rate of corrosion which is expressed by the current density, R is the universal gas constant in $\text{J mol}^{-1} \text{K}^{-1}$, T is the temperature in K and h is the Planck's constant. To obtain ΔH^* and ΔS^* , $\log i/T$ versus $1/T$ are plotted at different concentrations of AEO7 corrosion inhibitor as displayed in Fig. 10.

ΔH^* values are computed from the slopes of the plots while ΔS^* values are calculated from the intercept of the plots in Fig. 10. The computed values of E_a , ΔH^* and ΔS^* are presented in Table 7. Clearly, it is seen that ΔH^* values in the presence of AEO7 corrosion inhibitor are smaller than those for AEO7-free HCl solutions. In addition, raising the concentration of AEO7 increases E_a and ΔS^* values. This trend supports the physisorption mechanism which is proposed for the adsorption of AEO7 molecules on the C-steel surface in a 0.5 M HCl solution.

A similar interpretation can be made using the thermodynamic equation below^{30,84}:

$$RT = E_a - \Delta H^* \quad (21)$$

The values of ΔH^* are smaller compared to those of E_a . The ΔS^* values are large and negative. The ΔS^* value becomes less negative with increasing AEO7 concentration indicating a decline in the level of perturbation of the AEO7 molecule to move from the reactant state to the activated complex one⁸².

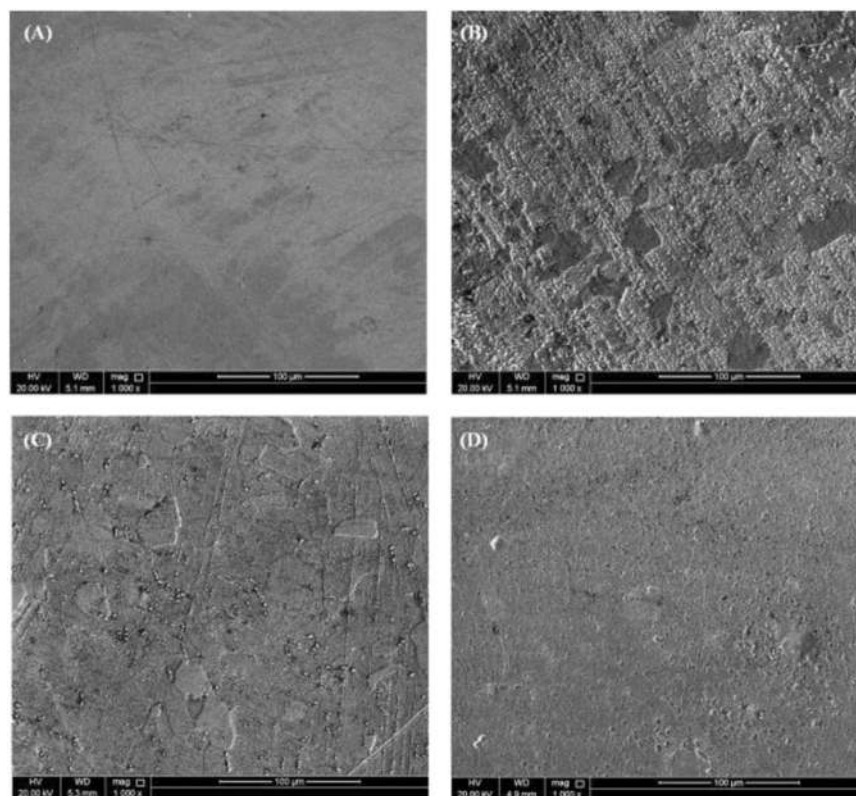


Figure 11. SEM micrographs for (A) a polished C-steel coupon in the (B) absence and (C) presence of $40 \mu\text{mol L}^{-1}$ of AEO7 alone and (D) in the presence of $1 \times 10^{-3} \text{ M}$ of KI along with $40 \mu\text{mol L}^{-1}$ of AEO7 in 0.5 M HCl medium.

$\Delta E_{\text{gap}}(\text{eV})$	$I(\text{eV})$	$A(\text{eV})$	$\gamma(\text{eV})$	$X(\text{eV})$	$\delta(\text{eV})$	$\mu(\text{D})$
8.21	6.89	-1.31	4.10	2.79	0.24	0.48

Table 8. Quantum chemical parameters of AEO7 calculated at the B3LYP/cc-pvdz level of theory

Microscope Analysis. Figures 11 and S2 compare the surface morphology of (A) a polished C-steel coupon using the SEM (Fig. 11) and optical profilometry (Figure S2) with another coupon after immersion for 24 h in 0.5 M HCl in the (B) absence and (C) presence of $40 \mu\text{mol L}^{-1}$ of AEO7 alone and (D) in presence of $1 \times 10^{-3} \text{ M}$ of KI along with $40 \mu\text{mol L}^{-1}$ of AEO7. The polished coupons did not exhibit any noticeable defects, except polishing scratches (Fig. 11A) with a surface roughness ($R_a = 0.02 \mu\text{m}$). After immersion in 0.5 M HCl without any inhibitor, heavy corrosion attack takes place (Fig. 11B) and R_a increases to $3.2 \mu\text{m}$. In Figs 11C and 13C, where the AEO7 corrosion inhibitor exists, the corrosion is decreased significantly compared with that in its absence (Figs 11B and S2B) and R_a decreases to $0.12 \mu\text{m}$. In presence of $1 \times 10^{-3} \text{ M}$ KI in addition to $40 \mu\text{mol L}^{-1}$ of AEO7, a synergistic effect take place as the surface look clean and R_a decreases significantly to $0.06 \mu\text{m}$.

AFM analysis. The three-dimensional AFM technique is one of the ideal approaches for exploring the surface topography at the nano and microlevels. It is also a powerful method for elucidating the efficiency of the corrosion inhibitor⁸⁴. The optical profilometry provides qualitative images at the microscale level. However, the quantitative details for the surface roughness of C-steel can be determined by AFM where the mean roughness factor (R_a) can be measured. The R_a values show that the roughness of C-steel immersed in 0.5 M HCl increases from 20 nm for the unexposed specimen to 320 nm for the coupon corroded in an uninhibited-HCl solution. However, the addition of $40 \mu\text{mol L}^{-1}$ of AEO7 reduces the R_a to 120 nm due to the formed adsorbed protective layer. Moreover, upon adding $1 \times 10^{-3} \text{ M}$ KI to the AEO7, the R_a is reduced to 65 nm. These results are clear in the AFM micrographs shown in Fig. 12. Both SEM and AFM measurements confirm the high corrosion $IE\%$ of AEO7 especially in the presence of KI.

Quantum Chemical Calculations. Figure 13 represents the optimized structure of the inhibitor as well as the corresponding frontier molecular orbitals namely HOMO and LUMO. The molecule consists of a polar part composed of alternative eight oxygen atoms and ethylene groups linked to a zigzag non-polar hydrocarbon. The population of the electron density is focused on the oxygen atoms suggesting that heteroatoms behave as

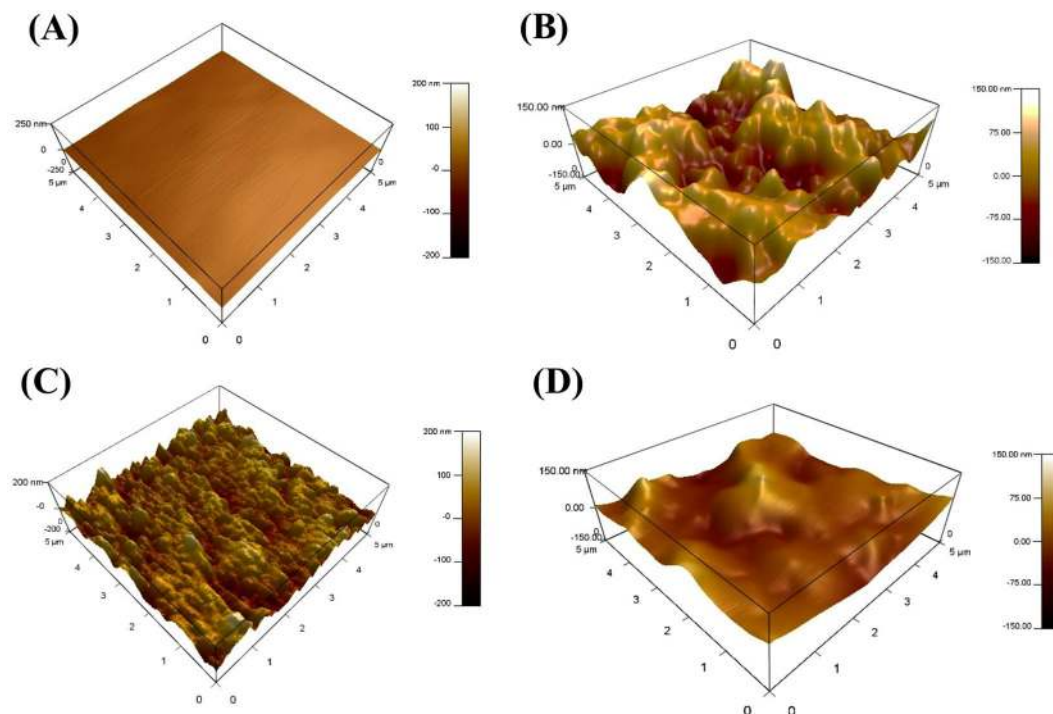


Figure 12. AFM images of (A) C-steel after polishing, in (B) absence, (C) presence of $40 \mu\text{mol. L}^{-1}$ of AEO7 corrosion inhibitor only and (D) in the presence of $1 \times 10^{-3} \text{ M KI}$ along with $40 \mu\text{mol L}^{-1}$ of AEO7 in 0.5 M HCl medium.

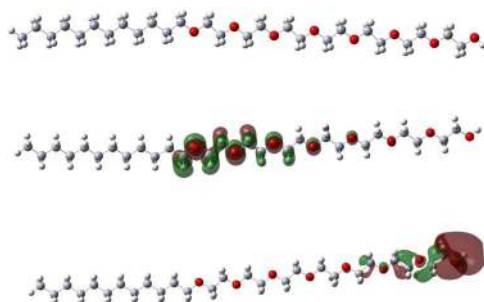


Figure 13. The optimized molecular structure of the AEO7 at the B3LYP/cc-pvdz level of theory (upper) and its frontier molecular orbital density distributions: (middle) HOMO and (lower) LUMO.



Figure 14. Mulliken charges of the AEO7 calculated at the B3LYP/cc-pvdz level of theory.

active sites with the highest ability to interact with the metal surface. The presence of these electronegative atoms increases the polarity of the molecule as well as their interaction with the charged sites on the metal surface enhancing the adsorption probability and then preventing interaction of the surface with the environment^{85,86}.

Figure 14 depicts the Mulliken charge distributions of AEO7. The highest electron densities are located at oxygen atoms ($\approx -0.34 \text{ au}$) indicating that oxygen atoms are the active centers, which have the strongest ability to interact of the metal surface. This finding is in line with the HOMO populations. This interaction with the metal surface with several numbers of active centers provides a good protective layer on the metal surface.

The quantum chemical parameters are calculated and listed in Table 8. The large energy gap decreases the ability of the inhibitor to form coordinate bonds with the d -orbital of the metal by donating and accepting electrons. Moreover, large global hardness and small global softness values reveal the inhibitor resistance to charge

transfer and decreased the ability to receive electrons. However, the polarity of the molecule as inferred from the value of the dipole moment suggests a good electrostatic interaction with the metal surface and in turn enhances the inhibition ability. Therefore, these results are in good agreement with the experimental data i.e. the inhibitor favors the physical adsorption on the metal surface⁸⁷.

Conclusion

AEO7 is an effective corrosion inhibitor for C-steel in 0.5 M HCl solutions. The presence of KI synergistically enhanced the corrosion *IE*% and the adsorption of AEO7 at the C-steel surface at ambient temperature. Weight loss results reveal a high corrosion *IE*% especially at room temperatures. EIS and polarization measurements confirm the adsorption of AEO7 corrosion inhibitor molecules on the C-steel surface and the formation of a protective layer that suppresses the C-steel oxidation and the hydrogen ion reduction reactions at the anodic and cathodic sites, respectively. AEO7 molecules are exothermically physisorbed on the C-steel surface, and the adsorption follows the Freundlich isotherm. SEM, optical profilometry and AFM measurements reveal a smooth surface of the C-steel coupon when immersed in an AEO7-inhibited HCl solution compared to the cases when an uninhibited HCl solution is used where severe corrosion takes place, which increases the surface roughness significantly.

Data Availability Statement

The raw data required to reproduce these findings can be shared at any time based on direct requests to the authors.

References

- L.D. Hanwei Liang, Hiroki Tanikawa, Ning Zhang, Zhiqiu Gao, Xiao Luo, Feasibility of a new-generation nighttime light data for estimating in-use steel stock of buildings and civil engineering infrastructures, *Resour. Conserv. Recycl.* **123** 11–23 (2017).
- A.A.D.S. Mohd Sayuti, Faheem Salem, Novel uses of SiO₂ nano-lubrication system in hard turning process of hardened steel AISI4140 for less tool wear, surface roughness and oil consumption, *J. Clean. Prod.* **67** 265–276 (2014).
- Bousskri, A. *et al.* Corrosion inhibition of carbon steel in aggressive acidic media with 1-(2-(4-chlorophenyl)-2-oxoethyl)pyridazinium bromide. *J. Mol. Liq.* **211**(Supplement C), 1000–1008 (2015).
- Deyab, M. A., Zaky, M. T. & Nessim, M. I. Inhibition of acid corrosion of carbon steel using four imidazolium tetrafluoroborates ionic liquids. *J. Mol. Liq.* **229**(Supplement C), 396–404 (2017).
- Verma, C., Quraishi, M. A., Ebenso, E. E., Obot, I. B. & El Assry, A. 3-Amino alkylated indoles as corrosion inhibitors for mild steel in 1M HCl: Experimental and theoretical studies. *J. Mol. Liq.* **219**(Supplement C), 647–660 (2016).
- Sastri, V. S. Green corrosion inhibitors: theory and practice (John Wiley & Sons, Hoboken, New Jersey, 2012).
- Stansbury, R. A. B. E. E. Fundamentals of electrochemical corrosion. *ASM Int.*, 271–277 (2000).
- Hojambardiev, M. *et al.* Hydrothermal-induced growth of Ca10V6O25 crystals with various morphologies in a strong basic medium at different temperatures. *Materials Research Bulletin* **48**(4), 1388–1396 (2013).
- Mohamed, A. M. A., Abdullah, A. M. & Younan, N. A. Corrosion behavior of superhydrophobic surfaces: A review. *Arabian Journal of Chemistry* **8**(6), 749–765 (2015).
- Radwan, A. B., Mohamed, A. M. A., Abdullah, A. M. & Al-Maadeed, M. A. Corrosion protection of electrospun PVDF–ZnO superhydrophobic coating. *Surface and Coatings Technology* **289**(Supplement C), 136–143 (2016).
- Sk, M. H. *et al.* Local supersaturation and the growth of protective scales during CO₂ corrosion of steel: Effect of pH and solution flow. *Corrosion Science* **126**(Supplement C), 26–36 (2017).
- Banerjee, S. S. & Singh, V. M. M. Chemically Modified Natural Polysaccharide as Green Corrosion Inhibitor for Mild Steel in Acidic Medium. *Corros. Sci.* **59**, 35–41 (2012).
- Gerengi, H. & Sahin, H. I. Schinopsis lorentzii Extract As a Green Corrosion Inhibitor for Low Carbon Steel in 1 M HCl Solution. *Ind. Eng. Chem. Res.* **51**(2), 780–787 (2012).
- Kumar, R., Yadav, O. S. & Singh, G. Electrochemical and surface characterization of a new eco-friendly corrosion inhibitor for mild steel in acidic media: A cumulative study. *J. Mol. Liq.* **237**(Supplement C), 413–427 (2017).
- Nnaji, N. J. N. *et al.* Morpholine and piperazine based carboxamide derivatives as corrosion inhibitors of mild steel in HCl medium. *J. Mol. Liq.* **230**(Supplement C), 652–661 (2017).
- Verma, C., Ebenso, E. E. & Vishal, Y. M. A. Quraishi, Dendrimers: A new class of corrosion inhibitors for mild steel in 1M HCl: Experimental and quantum chemical studies. *J. Mol. Liq.* **224**(Part B), 1282–1293 (2016).
- Hegazy, A. Y. E.-E. M. A., El-Shafaa, M. & Berry, K. M. Novel cationic surfactants for corrosion inhibition of carbon steel pipelines in oil and gas wells applications. *J. Mol. Liq.* **214**, 347–356 (2016).
- Zhu, M. L. F. Y. & Cho, J.-H. Integrated evaluation of mixed surfactant distribution in water-oil-steel pipe environments and associated corrosion inhibition efficiency. *Corros. Sci.* **110**, 213–227 (2016).
- Fakiha El-Taib, A. E. E. Heakal, Gemini surfactants as corrosion inhibitors for carbon steel. *J. Mol. Liq.* **230**, 395–407 (2017).
- Shaban, S. M., El-Sherif, R. M. & Fahim, M. A. Studying the surface behavior of some prepared free hydroxyl cationic amphiphathic compounds in aqueous solution and their biological activity. *J. Mol. Liq.* **252**, 40–51 (2018).
- Xu, H. J., Lu, C. X. & Ye, Z. W. Synthesis and properties of the kind of green surfactants. *Nanjing Li Gong Daxue Xuebao/Journal of Nanjing University of Science and Technology* **29**(1), 62–65 (2005).
- Wu, J., Cai, G., Liu, J., Ge, H. & Wang, J. Eco-friendly surface modification on polyester fabrics by esterase treatment. *Applied Surface Science* **295**, 150–157 (2014).
- Bianchetti, C. L. D. G. O. & Seddon, K. R. Bleaching systems in domestic laundry detergents: a review. *RSC Advances* **5**, 65365–65384 (2015).
- Arthur, J. R. H. T., Phan, L., Jessop, P. G. & Hodson, P. V. Effects-driven chemical design: the acute toxicity of CO₂-triggered switchable surfactants to rainbow trout can be predicted from octanol-water partition coefficients. *Green Chem.* **14**, 357–362 (2012).
- Abdallah, M. Ethoxylated fatty alcohols as corrosion inhibitors for dissolution of zinc in hydrochloric acid. *Corrosion Science* **45**(12), 2705–2716 (2003).
- Mobin, M. *et al.* Bio-/Environment-Friendly Cationic Gemini Surfactant as Novel Corrosion Inhibitor for Mild Steel in 1 M HCl Solution. *Journal of Surfactants and Detergents* **20**, 57–74 (2017).
- Samy, A. A. A.-E., Shaban, M. & Salah, M. T. Gravimetric and electrochemical evaluation of three nonionic dithiol surfactants as corrosion inhibitors for mild steel in 1 M HCl solution. *J. Mol. Liq.* **216**, 392–400 (2016).
- Zhanga, N. T. Z., Lia, X., Zhanga, L., Wuc, L. & Huang, Y. Synergistic inhibition behavior between indigo carmine and cetyl trimethyl ammonium bromide on carbon steel corroded in a 0.5 M HCl solution. *Applied Surface Science* **357**, 845–855 (2015).

29. Jokar, T. S. F. M. & Ramezanzadeh, B. Electrochemical and surface characterizations of *Morus alba* Pendula leaves extract (MAPLE) as a green corrosion inhibitor for steel in 1 M HCl. *J. Taiwan Inst. Chem. Eng.* **63**, 436–452 (2016).
30. Kowsari, S. Y. A. E. *et al.* *In situ* synthesis, electrochemical and quantum chemical analysis of an amino acid-derived ionic liquid inhibitor for corrosion protection of mild steel in 1M HCl solution. *Corros. Sci.* **112**, 73–85 (2016).
31. A. G1-90, Standard Practice for Preparing, Cleaning, and Evaluating Corrosion Test Specimens (1999).
32. Yadav, M., Gope, L., Kumari, N. & Yadav, P. Corrosion inhibition performance of pyranopyrazole derivatives for mild steel in HCl solution: Gravimetric, electrochemical and DFT studies. *J. Mol. Liq.* **216**(Supplement C), 78–86 (2016).
33. R.C. Gaussian 09, M. J. Frisch, G. W. Trucks, H. B. Schlegel, G. E. Scuseria, M. A. Robb, J. R. Cheeseman, G. Scalmani, V. Barone, B. Mennucci, G. A. Petersson, H. Nakatsuji, M. Caricato, X. Li, H. P. Hratchian, A. F. Izmaylov, J. Bloino, G. Zheng, J. L. Sonnenberg, M. Hada, M. Ehara, K. Toyota, R. Fukuda, J. Hasegawa, M. Ishida, T. Nakajima, Y. Honda, O. Kitao, H. Nakai, T. Vreven, J. A. Montgomery, Jr., J. E. Peralta, F. Ogliaro, M. Bearpark, J. J. Heyd, E. Brothers, K. N. Kudin, V. N. Staroverov, T. Keith, R. Kobayashi, J. Normand, K. Raghavachari, A. Rendell, J. C. Burant, S. S. Iyengar, J. Tomasi, M. Cossi, N. Rega, J. M. Millam, M. Klene, J. E. Knox, J. B. Cross, V. Bakken, C. Adamo, J. Jaramillo, R. Gomperts, R. E. Stratmann, O. Yazyev, A. J. Austin, R. Cammi, C. Pomelli, J. W. Ochterski, R. L. Martin, K. Morokuma, V. G. Zakrzewski, G. A. Voth, P. Salvador, J. J. Dannenberg, S. Dapprich, A. D. Daniels, O. Farkas, J. B. Foresman, J. V. Ortiz, J. Cioslowski, and D. J. Fox, Gaussian, Inc., Wallingford CT2010.
34. Lee, C., Yang, W. & Parr, R. G. Development of the Colle-Salvetti correlation-energy formula into a functional of the electron density. *Physical Review B* **37**(2), 785–789 (1988).
35. Becke, A. D. Density-functional thermochemistry. III. *The role of exact exchange*, *J. Chem. Phys.* **98**, 5648 (1993).
36. Thorn H, D. Jr. Gaussian basis sets for use in correlated molecular calculations. I. The atoms boron through neon and hydrogen. *J. Chem. Phys.* **90**, 1007 (1989).
37. Chong, D. P., Herring, F. G. & Takahata, Y. Prediction of large corrections to Koopman's theorem and the ab initio vertical potentials of HOCl, FOCl and Cl₂O. *Journal of Electron Spectroscopy and Related Phenomena* **13**(1), 39–47 (1978).
38. Koopmans, T. Über die Zuordnung von Wellenfunktionen und Eigenwerten zu den Einzelnen Elektronen Eines Atoms. *Physica* **1**(1), 104–113 (1934).
39. Aloui, I. F. S. *et al.* New mechanism synthesis of 1,4-benzothiazine and its inhibition performance on mild steel in hydrochloric acid. *Port. Electrochim. Acta* **27**, 599–613 (2009).
40. Foad El-Sherbini, S. M. A. W. E. E. & Deyab, M. Ethoxylated fatty acids as inhibitors for the corrosion of zinc in acid media. *Mater. Chem. Phys.* **89**, 183–191 (2005).
41. Kharbach, Y. *et al.* Anticorrosion performance of three newly synthesized isatin derivatives on carbon steel in hydrochloric acid pickling environment: Electrochemical, surface and theoretical studies. *J. Mol. Liq.*
42. Hameed, R. S. I. A., Omar, Eissa, M., Fayed & Ghanem, M. Raed, New non ionic polymeric surfactants as corrosion inhibitors for the C-steel alloy in hydrochloric acid corrosive medium. *Chemica Sinica* **3**, 236–248 (2012).
43. Aslam, R., Mobin, M., Aslam, J. & Lgaz, H. Sugar based N,N'-didodecyl-N,N'-digluconamide ethylenediamine gemini surfactant as corrosion inhibitor for mild steel in 3.5% NaCl solution-effect of synergistic KI additive. *Scientific Reports* **8**(1), 3690 (2018).
44. Parveen, M., Mobin, M., Zehra, S. & Aslam, R. L-proline mixed with sodium benzoate as sustainable inhibitor for mild steel corrosion in 1M HCl: An experimental and theoretical approach. *Scientific Reports* **8**(1), 7489 (2018).
45. Bahgat Radwan, A., Sliem, M. H., Okonkwo, P. C., Shibl, M. F. & Abdullah, A. M. Corrosion inhibition of API X120 steel in a highly aggressive medium using stearamidopropyl dimethylamine. *J. Mol. Liq.* **236**(Supplement C), 220–231 (2017).
46. El Faydy, M. *et al.* Experimental investigation on the corrosion inhibition of carbon steel by 5-(chloromethyl)-8-quinolinol hydrochloride in hydrochloric acid solution. *J. Mol. Liq.* **219**(Supplement C), 396–404 (2016).
47. Lgaz, H., Salghi, R., Jodeh, S. & Hammouti, B. Effect of clozapine on inhibition of mild steel corrosion in 1.0M HCl medium. *J. Mol. Liq.* **225**(Supplement C), 271–280 (2017).
48. Yadav, M., Sarkar, T. K. & Purkait, T. Amino acid compounds as eco-friendly corrosion inhibitor for N80 steel in HCl solution: Electrochemical and theoretical approaches. *J. Mol. Liq.* **212**(Supplement C), 731–738 (2015).
49. Tang, Y. *et al.* Novel benzimidazole derivatives as corrosion inhibitors of mild steel in the acidic media. Part I: Gravimetric, electrochemical, SEM and XPS studies. *Corros. Sci.* **74**, 271–282 (2013).
50. Singh, A. K., Shukla, S. K., Singh, M. & Quraishi, M. A. Inhibitive effect of ceftazidime on corrosion of mild steel in hydrochloric acid solution. *Mater. Chem. Phys.* **129**(1–2), 68–76 (2011).
51. Espinoza-Vázquez, A. *et al.* Electrochemical assessment of phenol and triazoles derived from phenol (BPT) on API 5L X52 steel immersed in 1 M HCl. *RSC Advances* **6**(77), 72885–72896 (2016).
52. Verma, C. *et al.* Corrosion inhibition of mild steel in 1M HCl by D-glucose derivatives of dihydropyrido [2,3-d:6,5-d'] dipyrimidine-2, 4, 6, 8(1H,3H, 5H,7H)-tetraone. *Scientific Reports* **7**, 44432 (2017).
53. Mansfeld, F. Use of electrochemical impedance spectroscopy for the study of corrosion protection by polymer coatings. *J Appl Electrochem* **25**(3), 187–202 (1995).
54. Valcarce, M. B. & Vázquez, M. Carbon steel passivity examined in solutions with a low degree of carbonation: The effect of chloride and nitrite ions. *Mater. Chem. Phys.* **115**(1), 313–321 (2009).
55. Ahamad, I., Prasad, R. & Quraishi, M. A. Adsorption and inhibitive properties of some new Mannich bases of Isatin derivatives on corrosion of mild steel in acidic media. *Corros. Sci.* **52**(4), 1472–1481 (2010).
56. Farag, A. A., Ismail, A. S. & Migahed, M. A. Inhibition of carbon steel corrosion in acidic solution using some newly polyester derivatives. *J. Mol. Liq.* **211**(Supplement C), 915–923 (2015).
57. Zhang, B. R. *et al.* Synergistic corrosion inhibition of environment-friendly inhibitors on the corrosion of carbon steel in soft water. *Corros. Sci.* **94**, 6–20 (2015).
58. Bouammali, H. *et al.* Anticorrosion potential of diethylenetriaminepentakis (methylphosphonic) acid on carbon steel in hydrochloric acid solution. *J. Ind. Eng. Chem.* **26**, 270–276 (2015).
59. Prajila, M. & Joseph, A. Inhibition of mild steel corrosion in hydrochloric using three different 1,2,4-triazole Schiff's bases: A comparative study of electrochemical, theoretical and spectroscopic results. *J. Mol. Liq.* **241**(Supplement C), 1–8 (2017).
60. Kumar, R., Chopra, R. & Singh, G. Electrochemical, morphological and theoretical insights of a new environmentally benign organic inhibitor for mild steel corrosion in acidic media. *J. Mol. Liq.* **241**(Supplement C), 9–19 (2017).
61. Lgaz, H. *et al.* Correlated experimental and theoretical study on inhibition behavior of novel quinoline derivatives for the corrosion of mild steel in hydrochloric acid solution. *J. Mol. Liq.* **244**(Supplement C), 154–168 (2017).
62. Shaw, B. A., McCosby, M. M., Abdullah, A. M. & Pickering, H. W. The localized corrosion of AI 6XXX alloys. *JOM* **53**, 42 (2001).
63. Kaczerewska, O. *et al.* Effectiveness of O-bridged cationic gemini surfactants as corrosion inhibitors for stainless steel in 3 M HCl: Experimental and theoretical studies. *J. Mol. Liq.* **249**, 1113–1124 (2018).
64. Zarrouk, A. *et al.* Inhibitive properties, adsorption and theoretical study of 3,7-dimethyl-1-(prop-2-yn-1-yl)quinoxalin-2(1H)-one as efficient corrosion inhibitor for carbon steel in hydrochloric acid solution. *J. Mol. Liq.* **222**(Supplement C), 239–252 (2016).
65. Amin, M. A., Khaled, K. F. & Fadel-Allah, S. A. Testing validity of the Tafel extrapolation method for monitoring corrosion of cold rolled steel in HCl solutions - Experimental and theoretical studies. *Corros. Sci.* **52**(1), 140–151 (2010).
66. Abd-Elaal, A. A., Elbasiony, N. M., Shaban, S. M. & Zaki, E. G. Studying the corrosion inhibition of some prepared nonionic surfactants based on 3-(4-hydroxyphenyl) propanoic acid and estimating the influence of silver nanoparticles on the surface parameters. *J. Mol. Liq.* **249**(Supplement C), 304–317 (2018).

67. Usman, B. J., Umoren, S. A. & Gasem, Z. M. Inhibition of API 5L X60 steel corrosion in CO₂-saturated 3.5% NaCl solution by tannic acid and synergistic effect of KI additive. *J. Mol. Liq.* **237**(Supplement C), 146–156 (2017).
68. Vashisht, H. *et al.* Synergistic interactions between tetra butyl phosphonium hydroxide and iodide ions on the mild steel surface for corrosion inhibition in acidic medium. *J. Mol. Liq.* **224**(Part A), 19–29 (2016).
69. Ramya, K. M., Anupama, K. K. & Joseph, A. Electrochemical and Theoretical Studies on the Synergistic Interaction and Corrosion Inhibition of Alkyl Benzimidazoles and Thiosemicarbazide Pair on Mild Steel in Hydrochloric Acid. *Mater. Chem. Phys.* **150** 632–647 (2015).
70. Aramaki, K. & Hackerman, N. *J. Electrochem. Soc.* **116**, 568 (1969).
71. Al-Fahemi, J. H., Abdallah, M., Gad, E. A. M. & Jahdaly, B. A. A. L. Experimental and theoretical approach studies for melatonin drug as safely corrosion inhibitors for carbon steel using DFT. *J. Mol. Liq.* **222**(Supplement C), 1157–1163 (2016).
72. Anusuya, N., Saranya, J., Sounthari, P., Zarrouk, A. & Chitra, S. Corrosion inhibition and adsorption behaviour of some bis-pyrimidine derivatives on mild steel in acidic medium. *J. Mol. Liq.* **225**(Supplement C), 406–417 (2017).
73. Seifzadeha, H. B. D., Bezaatpou, A. & Schiff, A. base compound as effective corrosion inhibitor for magnesium in acidic media. *Mater. Chem. Phys.* **138**, 794–802 (2013).
74. Zaaafarany, I. A. Corrosion inhibition of 1018 carbon steel in hydrochloric acid using Schiff base compounds. *International Journal of Corrosion and Scale Inhibition* **3**, 12–27 (2014).
75. Zeino, A., Abdulazeez, I., Khaled, M., Jawich, M. W. & Obot, I. B. Mechanistic study of polyaspartic acid (PASP) as eco-friendly corrosion inhibitor on mild steel in 3% NaCl aerated solution. *J. Mol. Liq.* **250**, 50–62 (2018).
76. Wanees, S. A. E., Bahgat Radwan, A., Alsharif, M. A. & Abd El, S. M. Haleem, Initiation and inhibition of pitting corrosion on reinforcing steel under natural corrosion conditions. *Materials Chemistry and Physics* **190**(Supplement C), 79–95 (2017).
77. Bouklah, M., Hammouti, B., Lagrenée, M. & Bentiss, F. Thermodynamic properties of 2,5-bis(4-methoxyphenyl)-1,3,4-oxadiazole as a corrosion inhibitor for mild steel in normal sulfuric acid medium. *Corros. Sci.* **48**(9), 2831–2842 (2006).
78. Esmaeili, N., Neshati, J. & Yavari, I. Corrosion inhibition of new thiocarbonylhydrazides on the carbon steel in hydrochloric acid solution. *J. Ind. Eng. Chem.* **22**, 159–163 (2015).
79. Hoseinzadeh, A. R. D., Maddahy, I., Avei, M. H. & Taurine, M. R. as a Green Corrosion Inhibitor for AISI 4130 Steel Alloy in Hydrochloric Acid Solution. *Chem. Eng. Commun.* **201**, 380–402 (2014).
80. Noor, E. A. A.-M. & Corrosion, A. H. Behavior of Mild Steel in Hydrochloric Acid Solutions. *Int. J. Electrochem. Sci.* **3**, 806–818 (2008).
81. S.S. Umoren, M. M., Israel, A. U., Eduok, U. M. & Jonah, A. J. Comparative Study of the Corrosion Inhibition Efficacy of Polypropylene Glycol and Poly(Methacrylic Acid) for Mild Steel in Acid Solution. *J. Dispersion Sci. Technol.* **36**, 1721–1735 (2015).
82. H.U. Gerengi, I., Solomon, M., Yildiz, M. & Goksu, H. Evaluation of the Inhibitive Effect of Diospyros kaki (Persimmon) Leaves Extract on St37 Steel Corrosion in Acid Medium. *Sustainable Chem. Pharm.* **4**, 57–66 (2016).
83. Shukla, S. K., Quraishi, M. A. & Prakash, R. A self-doped conducting polymer “polyanthranilic acid”: An efficient corrosion inhibitor for mild steel in acidic solution. *Corros. Sci.* **50**(10), 2867–2872 (2008).
84. Parul Dohare, K. R. A., Quraishi, M. A. & Obot, I. B. Pyranpyrazole derivatives as novel corrosion inhibitors for mild steel useful for industrial pickling process: Experimental and Quantum Chemical study. *J. Ind. Eng. Chem.* **52**, 197–210 (2017).
85. Kumar, R. *et al.* Corrosion inhibition performance of chromone-3-acrylic acid derivatives for low alloy steel with theoretical modeling and experimental aspects. *J. Mol. Liq.* **243**(Supplement C), 439–450 (2017).
86. Yadav, M., Sinha, R. R., Sarkar, T. K., Bahadur, I. & Ebseno, E. E. Application of new isonicotinamides as a corrosion inhibitor on mild steel in acidic medium: Electrochemical, SEM, EDX, AFM and DFT investigations. *J. Mol. Liq.* **212**(Supplement C), 686–698 (2015).
87. Srivastava, V. *et al.* Amino acid based imidazolium zwitterions as novel and green corrosion inhibitors for mild steel: Experimental, DFT and MD studies. *J. Mol. Liq.* **244**(Supplement C), 340–352 (2017).

Acknowledgments

This publication was supported by Qatar University Internal Grant N° GCC-2017-012. The findings achieved herein are solely the responsibility of the authors. The authors gratefully thank the Center for Advanced Materials at Qatar University and the Chemistry Department at Cairo University for their support. The permanent address of Dr. Mohamed F. Shibl is Chemistry Department, Faculty of Science, Cairo University, Giza 12613, Egypt.

Author Contributions

Mr. Mostafa and Mr. Afifi had the major contribution in the electrochemistry work and the manuscript writing equally but Mr. Mostafa's effort is higher in response to the reviewers' comments. Mr. Ahmed Bahgat Radwan and Dr. Eman Fayyad had their contributions in the surface characterization work and manuscript editing. Dr. Mohamed Shibl was responsible for all the theoretical part in this manuscript. Prof. Fakiha El-Taib Heakal and Dr. Aboubakr Abdullah are the team leaders at Cairo and Qatar Universities, respectively. They gathered everything, checked the data, discussed it and digested it in one manuscript.

Additional Information

Supplementary information accompanies this paper at <https://doi.org/10.1038/s41598-018-37254-7>.

Competing Interests: The authors declare no competing interests.

Publisher's note: Springer Nature remains neutral with regard to jurisdictional claims in published maps and institutional affiliations.



Open Access This article is licensed under a Creative Commons Attribution 4.0 International License, which permits use, sharing, adaptation, distribution and reproduction in any medium or format, as long as you give appropriate credit to the original author(s) and the source, provide a link to the Creative Commons license, and indicate if changes were made. The images or other third party material in this article are included in the article's Creative Commons license, unless indicated otherwise in a credit line to the material. If material is not included in the article's Creative Commons license and your intended use is not permitted by statutory regulation or exceeds the permitted use, you will need to obtain permission directly from the copyright holder. To view a copy of this license, visit <http://creativecommons.org/licenses/by/4.0/>.

© The Author(s) 2019